

Macroscopic-ranged proximity effect in graphite

Bruno Cury Camargo* and Piotr Gierłowski
*Institute of Physics, Polish Academy of Sciences,
Aleja Lotników 32/46, PL-02-668 Warsaw, Poland.*

Marek Kuzmiak
*Centre of Low Temperature Physics, Institute of Experimental Physics,
Slovak Academy of Sciences, 04001 Košice, Slovakia and
Faculty of Electrical Engineering and Informatics, Technical University, 04001 Košice, Slovakia*

Ramon Ferreira de Jesus
Instituto Federal do Rio Grande do Sul, Campus Vacaria, 952000-000 Vacaria, RS, Brazil.

Oleksandr Onufriienko and Pavol Szabó
*Centre of Low Temperature Physics, Institute of Experimental Physics,
Slovak Academy of Sciences, 04001 Košice, Slovakia*

Yakov Kopelevich
Instituto de Física Gleb Wattaghin, R. Sérgio Buarque de Holanda 777, 13083-859 Campinas, Brasil.
(Dated: January 18, 2022)

We report the induction of proximity-induced superconducting features over macroscopic lengths in highly oriented pyrolytic graphite (HOPG). The phenomenon is triggered when electrical currents are injected in the material through superconducting electrodes, few millimeters apart from each other. Such large range is anomalous, as proximity-induced features in normal conductors hardly surpass few micrometers. The results can be explained as due presence of pre-existing superconductivity in graphite on small, localized regions.

I. INTRODUCTION

When superconducting (S) and normal (N) materials are brought together, Cooper pairs from the S region drift into N. This is known as the superconducting proximity effect (PE), which causes a region of N close to the S-N interface to present superconductivity (SC). The effect occurs over distances of the order ξ_N , the normal coherence length in N. This value depends on the ratio between the superconducting coherence length in S (ξ_s) and the mean-free path of carriers in N (l). For the limiting cases $l \gg \xi_s$ and $l \ll \xi_s$ – the clean and dirty limits –, ξ_N assumes the form $\xi_N = \hbar v_F / 2\pi k_B T$ and $\xi_N = \sqrt{\hbar v_F l / 6\pi k_B T}$, respectively,¹ with v_F the Fermi velocity in N.

Although usually confined to regions tenths or hundredths of nanometers near the S-N interface, in some cases, the PE can occur over several thousand times the length ξ_N . This is observed in selected S-N-S systems, and is related mostly to the properties of the N material. In underdoped cuprates, for example, such a behavior has been tentatively attributed^{2–4} to the occurrence of superconducting fluctuations above T_c . In clean transition-edge sensors, on the other hand, the survival of the PE over scales thousands of times higher than ξ_N is thought to happen due to the presence of nonequilibrium superconductivity^{5,6}. In addition, geometrical quantization of superconducting excitations in clean N materials can protect supercurrents over length scales much above

ξ_N (see, e.g.^{7,8}).

One possibility to obtain the PE over macroscopic scales, hence, is to study the properties of S-N-S sandwiches with clean N materials possessing both large ξ_N and indications of superconducting fluctuations. A promising candidate satisfying both conditions is graphite, which can be described as a quasi-compensated layered semimetal. In this material^{9–11}, $\rho_a / \rho_c < 10^{-4}$, $l \lesssim 10 \mu\text{m}$ and $v_F \approx 10^6$ m/s. These values lead to large estimated normal coherence lengths at low temperatures $\xi_N(T = 4 \text{ K}) = \hbar v_F / 2\pi k_B T \approx 2 \mu\text{m}$. It also presents various indications of SC, reported across the literature. Among them, are the presence of switching features in magnetoresistance akin to Josephson junction arrays^{12–15}, signatures of a Bose-metal phase^{16,17} (also seen in Bi) and the existence of superconducting-like magnetization hysteresis loops even at high temperatures¹⁷. In addition, very recently, percolative ($R = 0$) superconductivity has been measured in twisted bi-¹⁸ and multi-layer¹⁹ graphenes.

Given these signatures, it is conceivable the superconducting PE in graphite can have a far longer reach than $\xi_N \approx 1 \mu\text{m}$, possibly reaching macroscopic scales. So far, however, no such a phenomenon has been observed. Instead, most available reports on the literature focus on nanometer-sized devices^{20–24}. Here, we studied the electrical transport characteristics of millimetric samples outfitted with superconducting current-injection leads. Results revealed signatures of a long-range PE in our devices, persisting above $700 \mu\text{m}$ ($200 - 300 \xi_N$) from the

superconducting electrodes - an unusually long distance in bulk systems.

II. RESULTS AND DISCUSSION

A. Sample preparation

All our samples were extracted from a commercially-available highly oriented pyrolytic graphite (HOPG) crystal with 0.3° mosaicity²⁵. Its room-temperature in-plane resistivity was, approximately, $5 \mu\Omega\cdot\text{cm}$. The devices had typical in-plane dimensions of $5 \text{ mm} \times 1 \text{ mm}$ and thicknesses varying between 0.15 mm and 0.4 mm .

Samples were either contacted in a standard 4-probe configuration for electrical transport measurements, or in a 6-probe Hall bar configuration for simultaneous Hall and longitudinal resistance measurements. Samples contacted in a 4-probe configuration had voltage electrodes covering the whole sample's surface width, as is schematized in the inset of Fig. 1. This was done to mitigate possible effects of current distribution in the material. Voltage electrodes of samples contacted in the 6-probe Hall bar configuration were spread across the whole height of the sample, for the same reasons (see Fig. 5).

Additional devices were prepared in a 8-probe longitudinal/Hall-bar hybrid configuration. In it, electrodes were placed at the surface and edges of the samples. This geometry was realized to verify possible current distribution issues. In these devices, edge electrodes covered the whole sample height (as for devices with 6 probes), whereas top electrodes were point-like (see Fig. 8).

B. Control samples and the superconducting alloy

Control samples were characterized in the interval $2 \text{ K} \leq T \leq 10 \text{ K}$ with all electrodes made of silver paste. Measurements revealed a smooth metallic-like behavior, typical of well-graphitized HOPG^{26–28}. Results are presented in Fig. 1.

Subsequent samples were contacted as indicated in the cartoon of Fig. 1, with two outermost electrodes composed of a superconductor (SC) and the remaining ones of silver paste. The distance between adjacent electrodes was approximately 0.7 mm to 1 mm . We refer to their contacts by the numbers shown in Fig. 1.

In total, ten samples were studied (labeled *GS1* to *GS10*). The electrical resistivity of our devices was probed with DC and low-frequency AC measurements (up to $f \approx 5 \text{ Hz}$), which yielded the same results. Experiments were simultaneously performed in two- and four- probe configurations. Two-probe measurements ($2p$) were achieved by applying current and measuring voltage between superconducting electrodes 1 and 4. Experiments in the four-probe configuration ($4p$) were performed by applying electrical current between (supercon-

ducting) contacts 1 and 4 and measuring the potential between the (normal) probes 2 and 3.

The superconductor chosen for the current electrodes was an alloy of In/Pb (50% in volume each) with critical temperature $T_c \approx 6.8 \text{ K}$ and critical magnetic field $B_c(0) < 1.8 \text{ T}$ (see the suppl. material for details). The alloy was connected to the edges of our samples with a soldering iron at 300° C . Thin copper wires attached the sample to the instrumentation.

C. Transport measurements

The main result of the present work is illustrated in Fig. 1. In it, resistance vs. temperature plots of the sample *GS1* are shown. Measurements were carried out prior and after connecting SC current-injection leads to the device. While no anomaly was observed for a sample with only N electrodes, the injection of electrical currents through SC contacts induced a superconducting-like transition in $4p$ measurements. This occurred despite voltage probes being distant ca. $0.7 \text{ mm} - 1 \text{ mm}$ from the SC contacts (two orders of magnitude above ξ_N). Such a behavior was shared by all our devices.

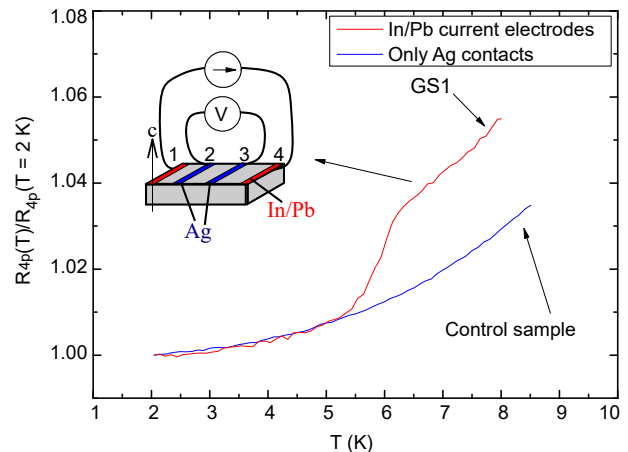


FIG. 1: Normalized four-probe $R_{4p}(T)$ curves for the control (pristine) graphite sample (blue curve) and for the device *GS1* (red curve) at zero magnetic field. The normalization factors were $R_{4p}(T = 2 \text{ K}) = 3.66 \text{ m}\Omega$ for the control and $R_{4p}(T = 2 \text{ K}) = 4.34 \text{ m}\Omega$ for *GS1*. The inset shows a sample schematic. Numbers 1 – 4 identify each electrode. The control sample was measured as indicated for *GS1*, but with all contacts made of non-superconducting silver paste.

The details of the $4p$ feature were sample dependent. In eight of our devices, the transition manifested as a sharp decrease of the $4p$ resistance ($R_{4p} \equiv V_{4p}/I$, I the applied current) below T_c . In one sample, it manifested as a sharp increase. One device did not present signatures of the $4p$ transition, within experimental uncertainty. When a decrease was observed, it accounted for, at most, 10% of the sample resistance at the center of

the transition. Its general behavior was similar to the one observed in $2p$ measurements ($R_{2p} \equiv V_{2p}/I$), which are undoubtedly associated to the superconductivity at the SC electrodes. The large distances between the normal and superconducting contacts in the $4p$ configuration, however, do not allow for the same interpretation. In what follows, we consider data of the majority of devices, showing a sharp decrease in $R_{4p}(T < T_c)$. The discussion, however, can also be applied to the case when a sharp increase manifests.

Figure 2 shows the behavior of sample *GS2* in the presence of in-plane magnetic fields ($B \perp c$) for the $2p$ and $4p$ configurations. This orientation was chosen to suppress the high orbital magnetoresistance of graphite, which can reach 1000 % for relatively low (≈ 0.1 T) magnetic fields along the material's c -axis¹¹. Because the phenomenon of interest was superimposed to this response, the chosen geometry ensured the best possible experimental resolution. Similar results were obtained for $B//c$ and are shown in the suppl. material. In the sample, the electrical current leads presented a contact resistance $R_C \approx 12.5$ m Ω at $T = 2$ K, while graphite ($R_{2p} - 2R_C$) had a resistance of approx. 32.3 m Ω . Two-probe measurements revealed a clear superconducting transition with $T_c \approx 6.8$ K, accounting for up to 6% of the total sample resistance at zero magnetic field. A transition was also observed in $4p$ measurements in the same temperature range, albeit accounting for up to 3% of the measured signal.

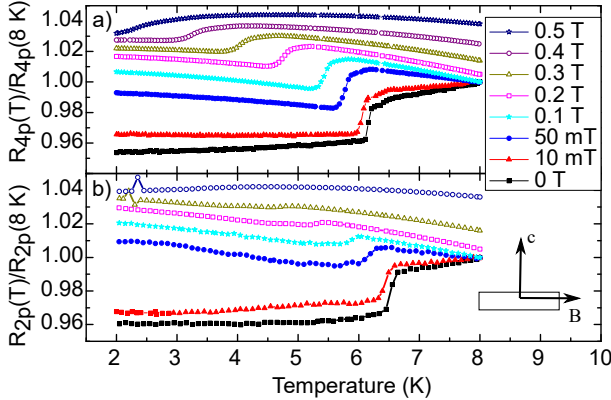


FIG. 2: a) 4-probe and b) 2-probe resistance of sample *GS2* as a function of temperature for different magnetic fields. The resistance has been normalized by its value in 8 K and the curves have been displaced vertically for clarity. The sample was measured as shown in the cartoon in fig. 1, with the magnetic field applied parallel to the graphene planes.

The amplitude of the $4p$ transition, defined as $\Delta R_{4p} \equiv |R_{4p}(T \lesssim T_c) - R_{4p}(T \gtrsim T_c)|$ (see fig. 3), did not vary monotonically as a function of B . Instead, it increased with the applied magnetic field, reaching saturation above 0.1 T (see Fig. 3). This behavior can be understood by considering the creation of a low-resistance channel below T_c , which operates in parallel with gra-

phite. The equivalent circuit is represented as a cartoon in Fig. 3. In it, the low resistance channel (denoted by R_s) acts as a shunt resistor, which carries a fraction I_s of the total electrical current I_0 applied to the system. Assuming that R_{4p} senses mostly the dissipative channel of graphite, the *measured* resistance below T_c can be expressed as a function of I_s by

$$R_{4p}(T < T_c) \equiv \frac{V_{4p}(T < T_c)}{I_0} = \frac{R(T) \times (I_0 - I_s)}{I_0}, \quad (1)$$

where $V_{4p}(T < T_c) = R(T) \times (I_s - I_0)$ corresponds to the actual *measured* voltage drop between normal electrodes on the sample, and $R(T)$ is the resistance of pristine graphite with normal electrodes.

Above T_c , $R_{4p}(T)$ should match the resistance of the pristine sample, as the low resistance channel ceases to exist ($I_s = 0$). In this case $R_{4p}(T > T_c) = R(T) \times I_0$ and, through eq. 1, we obtain a simple expression for the amplitude of the $4p$ transition

$$\Delta R_{4p} \equiv R_{4p}(T \lesssim T_c) - R_{4p}(T \gtrsim T_c) \approx R(T_c) \times \frac{I_s}{I_0}. \quad (2)$$

Considering the weak slope on the $R(T)$ behavior of pristine graphite (see Fig. 1), $R(T_c)$ is approximated by $R(T_c) \approx R_{4p}(T \gtrsim T_c)$. The expression 2 can then be normalized, resulting in

$$\frac{\Delta R_{4p}}{R_{4p}(T \gtrsim T_c)} \approx \frac{I_s}{I_0} \propto I_s \quad (3)$$

and providing a link between ΔR_{4p} and I_s .

We first consider the behavior of $\Delta R_{4p}/R$ at weak magnetic fields $B < 0.1$ T (see fig. 3c). In this field range, our data can be described with the circuit shown in Fig. 3b by assuming a low resistive channel $R_s \ll R$ weakly affected by small values of B , and I_s being limited by some interface resistance r . In this case $I_s = \Delta R_{4p}/[R_{4p}(T > T_c)] \approx 3R/(3R + 2r)$. The expression describes well the experimental data if we take r constant and $R \propto B^{1.2}$, which is the typical magnetoresistance of graphite¹¹.

At higher magnetic fields, on the other hand, the decay observed for $\Delta R_{4p}/R \propto I_s$ indicates a progressive suppression of the low resistance channel by B . In this field range, I_s has the functional form $I_s \propto \exp(-B/B_0)$. This is the same dependency expected for the critical current density through a thick superconductor-metal-superconductor Josephson junction with increasing magnetic fields²⁹, further suggesting the $4p$ transition as a superconducting proximity-induced feature in our system. The extracted parameter B_0 was $B_0 \approx 0.13$ T. This value practically coincides with the critical magnetic field $B_{crit} \approx 0.11$ T introduced in Ref.¹³, which corresponds to the magnetic field necessary to suppress the bosonic character of carriers in graphite. In other words, magnetic fields in this scale have been proposed to destroy electron-electron pairing in the system¹³.

Although the amplitude of the $4p$ anomaly did not change monotonically with T , the temperature in which

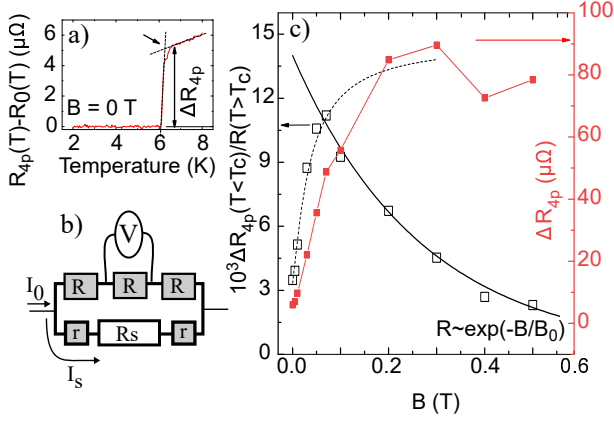


FIG. 3: a) Example of how the transition amplitude ΔR_{4p} was determined. The y-axis corresponds to R_{4p} of sample *GS2* at zero magnetic field after subtraction of a polynomial resistance background $R_0(T)$. ΔR_{4p} is chosen at the point indicated by an arrow in the figure. This value corresponds to the intersection between the maximum slope during the transition and a linear extrapolation of the R_{4p} behavior above T_c . b) Cartoon representing the proposed equivalent circuit for the sample. Below T_c , a low resistance channel R_s forms, which carries a fraction I_s of the total applied current I_0 . This results in a step of amplitude $\Delta R_{4p} = \Delta V/I_0 = R(T_c) \times I_s/I_0$, where $R(T_c)$ is the resistance of a pristine sample at T_c . c) Normalized (open symbols, left axis) and non-normalized (right axis, closed symbols) amplitude of the $4p$ transition as a function of the magnetic field in the device *GS2*. The dashed and solid lines are functions of the type $y = \alpha R/(r + R)$ and $y = \beta \exp(-B/B_0)$, respectively. On them, $R = (35 + 6.7 \times 10^4 B^{1.2})$ m Ω , $r = 50$ m Ω and $B_0 = 0.13$ T.

it occurred was displaced by the presence of magnetic fields according to the empirical expression

$$B_c(T) = B_c(0) \left(1 - \frac{T}{T_{c0}} \right), \quad (4)$$

which correlates the transition temperature T_c with the applied field B_c . In the equation, $B_c(0)$ corresponds to the critical magnetic field at $T = 0$ K, and T_{c0} the critical temperature at zero magnetic field.

The $B_c(T)$ diagrams for sample *GS2* are shown in Fig. 4. They revealed that the $4p$ feature happened at lower temperatures and magnetic fields in relation to the $2p$ transition. This result suggests the $4p$ transition as a consequence of the $2p$ one. Indeed, both $2p$ and $4p$ measurements revealed two transitions occurring in close proximity, which can be linked to the existence of two phases in the SC electrodes, with similar T_c 's (see the suppl. material). The persistence these features in $4p$ measurements indicate that the suppression of the $4p$ transition by magnetic fields is closely related to the suppression of superconductivity at the current electrodes³⁰. This is also reinforced by the fact that the B_c vs. T diagram for the $4p$ transition remained unchanged after modifying the

magnetic field orientation relative to the sample's c-axis (see the suppl. material). Such a result strengthens the hypothesis of superconducting electrodes as the objects inducing the phenomenon at hand. It also shows that the magnetic flux through the regions of HOPG responsible for the $4p$ transition does not depend on the magnetic field orientation. In a highly anisotropic system such as graphite, the latter can be explained by a low resistance channel confined to low-dimensional (quasi-1D or quasi-0D) sites/structures within the material.

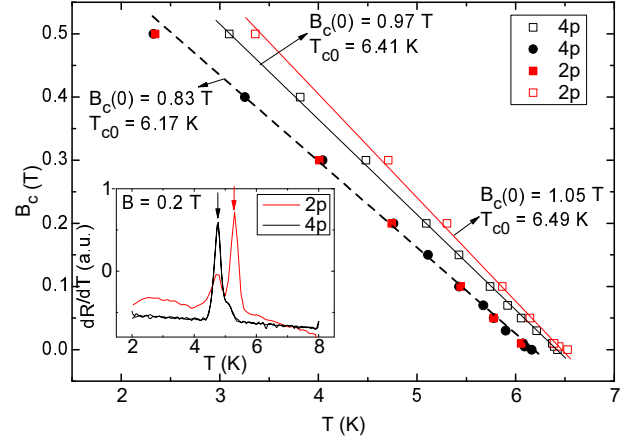


FIG. 4: $B_c(T)$ vs. T diagram of sample *GS1* for the $2p$ (red symbols) and $4p$ (black symbols) transitions. Open and closed symbols refer to subsequent transitions from the same $R(T)$ curve, happening at higher and lower temperatures, respectively. The lines follow from eq. 4 using the parameters $B_c(0)$ and T_{c0} shown in the figure. The inset shows the derivative of the $2p$ and $4p$ resistance as a function of temperature. The maxima in such curves were chosen as the transition temperature.

The existence of these regions/structures would also explain the behavior of $R_{4p}(T)$ in our devices, which did not show a continuous drop below T_c when compared with pristine samples (see Fig. 1). Such a result is at odds with the conventional superconducting PE. In it, the $4p$ resistance should change linearly with ξ_N , roughly^{1,31} as $R_{4p}(T) \propto R_0(1 - \kappa \xi_N)$, $\kappa \xi_N \propto 1/T$. Instead, our $R(T)$ results suggest that an eventual proximity-induced state seen in $4p$ must be confined to a fixed fraction of the sample volume, as also inferred from measurements performed at $B \perp c$ and $B // c$. This hypothesis is further supported by measurements in samples contacted in the $6p$ -Hall configuration, see fig. 5. On them, the resistance drop below T_c , observed in the longitudinal resistance, was larger than on other configurations (ranging about 10% of the total measured signal). Meanwhile, a negligible change in the Hall effect was observed in the same temperature range. Such results are consistent with the induction of the phenomenon at small, localized puddles on the sample, which usually do not contribute to the material's Hall conductivity.

The absence of the *conventional* superconducting PE

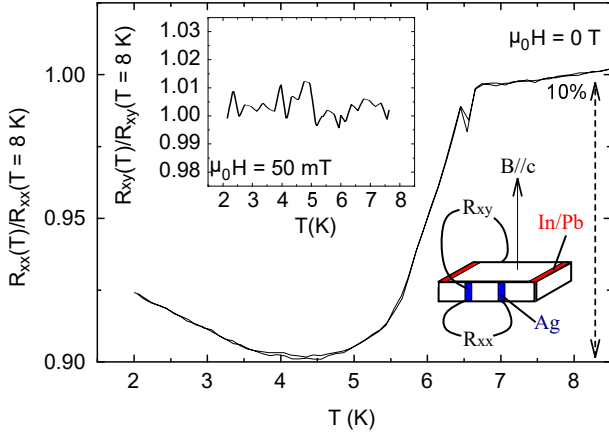


FIG. 5: Longitudinal resistance normalized by its value at $T = 8$ K for sample *GS5*, measured at zero magnetic field. The sample was contacted at the edges in a 6-probe Hall configuration, as shown in the cartoon. The inset shows the Hall resistance extracted at $B = 50$ mT, also normalized by its value at 8 K. Note the lack of a transition in the Hall component of resistance.

in our samples is further evidenced by experiments in asymmetric devices with a single superconducting electrode. Measurements in this configuration did not present any anomaly (see Fig. 6). These results also weight against experimental artifacts due to the distribution of electrical currents. Had this been the case here, the presence of a single superconducting electrode should suffice to prompt changes near at least one of the voltage probes, therefore, triggering the same effect seen in *4p*.

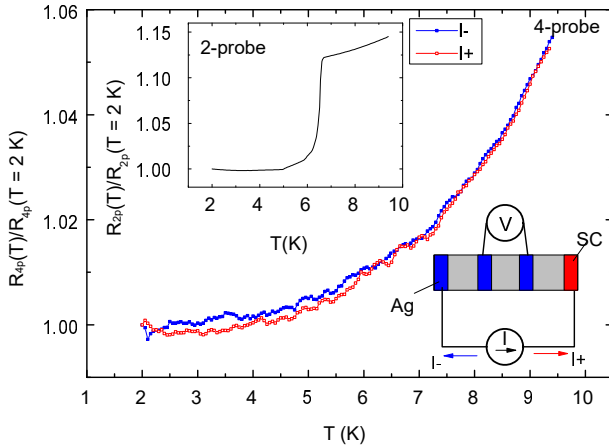


FIG. 6: Normalized resistance vs. temperature for a graphite sample contacted in an asymmetric configuration (only one superconducting electrode). Curves in the main panel show DC measurements, performed using different electrical current polarities. The cartoon on the bottom right illustrates how the experiment was performed. The inset shows data obtained in the *2p* configuration.

D. Surface characterization

We proceed to verify if our observations could be an artifact caused by the diffusion of superconducting material throughout graphite, originating from the current electrodes, or due to the dispersion of a “cloud” of superconducting particles across the sample surface during soldering.

Both possibilities are unlikely due to the characteristic time lengths involved in the soldering process (few seconds) and to the fact that no flux is used (hence, no “particle cloud” should form). For confirmation, scanning electron microscopy (SEM) measurements and extensive low-temperature scanning tunneling spectroscopy (STS) at different points across sample surfaces were carried out. Superconducting dust splattered during soldering should be observable in SEM images as small particles. Diffusion of superconducting material throughout graphite should manifest as superconducting gaps of amplitude ≈ 1 meV (the same one of lead) on scanning tunneling spectra measured over large sections of HOPG. Neither of these features were observed. In particular, scanning tunneling microscopy (STM) measurements in HOPG did not show qualitative differences above and below its electrode’s T_c . Combined, these observations categorically discard In/Pb diffusion or localized foreign superconducting islands as the source of our observations. Examples of SEM images of the sample surface, together with typical STM spectra are shown in fig. 7.

Despite not showing signatures of superconductivity, STS did reveal features similar to those of graphite/graphene. These include occasional regions with graphene-like spectra, periodic peaks on the density of states as a function of bias voltage and small pseudo-gap-like features, with energies in the range of 10 meV (see Fig. 7c,d). The latter have been previously observed and were associated with van-Hove singularities caused by the twisting of adjacent graphene layers. The obtained gap width (10 meV) corresponds to a rotation between layers³² around 1.13° . This value is close to the “magic angles” for which bilayer graphene has been recently reported to present superconductivity³³. Such a result provides a candidate for the localized regions subject to induced superconductivity in our samples.

Additionally, STM measurements made in the contact regime (i.e., the probing tip was touching graphite’s surface) presented zero bias conductance peaks in some regions of the sample surface. They manifested as a nearly two-fold enhancement of the local differential conductance in graphite. Such a feature was well-described within the Blonder-Tinkham-Klapwijk model for a direct ballistic N-S point contact junction³⁴. This feature, which is shown in the supplementary material, will be discussed in more detail elsewhere. Such results suggests the possibility of Andreev reflections of quasiparticles in a ballistic microstriction between a normal metal and a superconducting region, occurring during measurements in different parts of the sample.

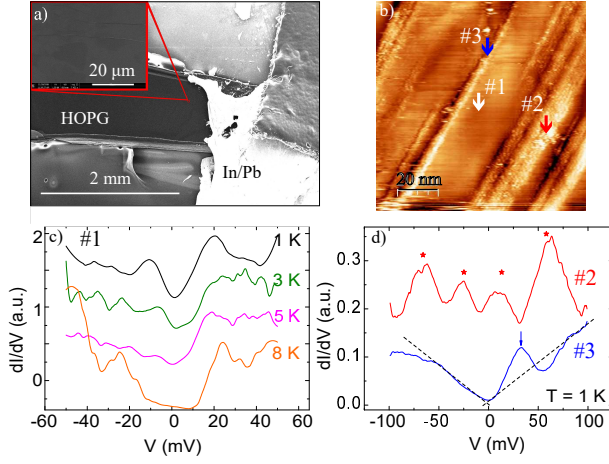


FIG. 7: a) SEM micrograph of a HOPG sample with a soldered In/Pb electrode (white area). The magnification corresponds to a $50 \mu\text{m} \times 50 \mu\text{m}$ region c.a. $200 \mu\text{m}$ distant from the superconducting electrode. No scattered material is observed. b) Typical topography of the region between electrodes for the graphite samples. The topography was measured at $T = 1 \text{ K}$ in an STM microscope. The arrows #1, #2 and #3 point the regions where the curves in c) and d) were obtained. c) Typical non-featureless differential conductance curves obtained in flat regions of STM scans. Curves have been displaced vertically for clarity. A gap-like structure is observed at low temperatures, which is not suppressed as T increases. d) Typical differential conductance features obtained at buckled (#2) and step regions (#3) at $T = 1 \text{ K}$. The peaks in #2, indicated by stars, are nearly periodic in V and can be associated to a pseudomagnetic field of 2.7 T assuming an electronic effective mass for graphite $m \approx 0.05m_e$, m_e the free electron mass³⁵. The straight lines in #3 are a guide to the eye, and indicate a graphene-like linear energy dispersion near the Fermi level³². The peak pointed by an arrow occurs around 30 mV and is associated to edge states of zig-zag terminated graphene flakes³⁶.

E. Current distribution

In anisotropic materials (such as graphite), contact placement can aggravate current distribution issues. These, in turn, can cause artifacts that compromise measurements. In this work, we minimize possible artifacts arising from current distribution by choosing different contact configurations/geometries, by measuring several devices, and by probing different samples.

As explained in Sec. II A, samples were contacted with three different probe configurations. Two of those are represented in figs. 1 and 5. Namely, samples with 4 probes were measured as schematized in the insert of fig. 1, with electrodes spanning the whole width of the sample. Conversely, samples contacted in the 6-probe Hall configuration (Fig. 5) had voltage electrodes placed only at the sample's edges, covering its entire height. Yet, in both cases, a clear transition to a lower resistance state was observed below T_c (see Figs. 1, 2 and 5).

The same qualitative behavior in both 4-probe and 6-probe-Hall geometries indicate that our samples are not subject to current distribution issues. Otherwise, qualitatively different results would be expected, hinging on contact positioning. This argument is supported by measurements performed in samples containing a single superconducting electrode. Results for one of these devices are shown in Fig. 6. All samples measured in this configuration (three in total, see the Suppl. material) did not present transitions below T_c . Had the origin of the $4p$ transition been associated with current distribution caused by the SC electrodes, it should also manifest on those samples.

Despite all our samples being prepared using the same raw materials, measurements performed on the 4-probe and 6-probe-Hall configurations, as shown in Figs. 2 and 5, were realized on different devices. To account for this, a sample was prepared in an 8-probe hybrid configuration. This geometry was a combination of the 4-probe and 6-probe Hall geometries, thus allowing the simultaneous measurement of the longitudinal $4p$ sample resistance at the top and along the edges of the sample. A schematic is shown on the inset of Fig. 8. Due to conservation of charge, current distribution issues on this device would require qualitatively different behaviors to be observed on different electrodes. Instead, simmilar measurements were obtained for both top and edge electrodes, corroborating the results presented in figs. 2 and 5. Such a result further discards current inhomogeneities as the source of the $4p$ transition reported here.

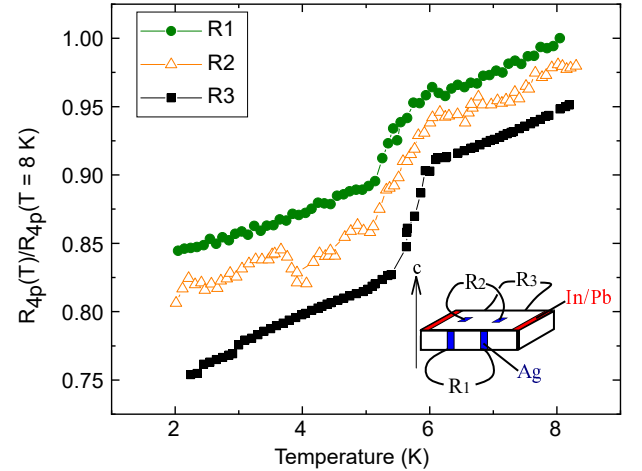


FIG. 8: Normalized $R_{4p}(T)/R_{4p}(T = 2K)$ measurements for a sample prepared with 8 electrodes (GS10), as represented in the inset of the figure. The current electrodes were made of a Pb/In alloy, whereas all voltage electrodes were composed by Ag paste. $R1$, $R2$ and $R3$ correspond to the respective electrode pairs shown in the inset. The normalizing factors were $R_{4p}(T = 2K) = 7 \mu\Omega$, $3 \mu\Omega$ and $13 \mu\Omega$ for $R1$, $R2$ and $R3$, respectively. $R2$ and $R3$ were measured along the sample edges, whereas $R1$ was measured at the sample top.

Finally, we verified possible instabilities of the instru-

mentation used during the experiments. For this, a piece of copper was probed under the same conditions as used for graphite samples. Results did not reveal any transitions (see the supplementary material), discarding instrumentation artifacts from current sources, amplifiers and voltmeters as the source of our observations in graphite.

F. Discussion

The overall behavior of the $4p$ transition triggered in graphite supports the presence of induced superconducting features in our devices in ranges above those of the conventional superconducting PE. Its characteristics, however, do not point towards a bulk-related phenomenon.

As discussed in section II C, the properties of our samples can be described by the existence of two independent transport channels acting in parallel: a high- and a low-resistance one. The high resistance channel seems to be related to transport through pristine graphite, whereas the low resistance channel is unambiguously associated to the presence of superconducting electrodes in the device. The fact that Hall measurements remain unchanged above and below T_c , whereas the sample's longitudinal resistance shows variations as large as 10%, strongly suggests that transport through the low resistance channel occurs along small localized grains in graphite, which should not contribute to its Hall resistance.

Suitably, the occurrence of the *conventional* superconducting PE does not justify the $4p$ transition. As previously presented, the lack of features in samples with a single SC electrode, the null dependence on T , the increasing transition amplitude with magnetic fields, and the long range of the phenomenon (up to $700\ \mu\text{m}$ - $1\ \text{mm}$ distant from the superconducting electrodes, whereas $\xi_N \approx 1 - 2\ \mu\text{m}$ ^{1,9-11,37-39}) all attest against such a hypothesis.

Instead, all our results can be accounted for by considering the pre-existence of mesoscopic, superconducting-prone islands in graphite. This hypothesis is consistent with previous reports in the literature, which indicate localized superconducting domains in the material^{12,14-16,40}. In this context, the presence of superconducting leads can act as a trigger for global coherent transport along such a pre-existing channel. In addition to overall sample behavior, superconducting puddles can be justified by point contact measurements performed during our STM study. These provided strong indications of Andreev reflections across graphite's surface, signaling the existence of superconducting regions in bulk HOPG with dimensions above the superconducting coherence length⁴¹.

Pristine samples, however, showed no superconducting-like transitions, in agreement with most reports to date^{11,17,21,42,43}. Such an observation requires that the transfer of charge from bulk graphite to the hypothesized superconducting regions must be forbidden under normal conditions. This can be justified

self-consistently when considering the superconducting islands in graphite as objects with reduced dimensions that are embedded in a quasi-2D electron gas with low conductance. This hypothesis has been suggested on previous STM, magnetization and transport studies in different types of pristine graphite^{12,14-16,27}, as well as inferred from our measurements.

Indeed, considering the typical $4p$ sample resistivity around $\sigma \approx 5\ \mu\Omega\cdot\text{cm}$ (see Fig. 1) and assuming a homogeneous current distribution across the sample volume, our devices show a conductance per graphene layer of the order $\sigma_L = \sigma c_0/t \approx 4.6 \times 10^{-4}\ \text{S} \approx 6G_0$. In it, $c_0 = 0.335\ \text{nm}$ is the interplane distancing in graphite, $t \approx 0.2\ \text{mm}$ the sample thickness and $G_0 = 2e^2/h$. In this case, the system could be roughly described as an array of superconducting islands at $T \ll T_c$, embedded in a quasi-2D electron gas (2DEG) with local conductance close to the conductance quantum. This situation is similar to a graphene film decorated with superconductors, tuned near the charge neutrality point³⁰. Under such circumstances, the Coulomb blockade impeding the introduction of carriers into the superconducting islands is expected to decrease with the conductivity of the 2DEG, following $\exp(-\pi^2 G_D/8)$, G_D the conductance of the metallic matrix^{44,45}. Such an enhanced Coulomb blockade at low conductances (approaching a few kilo Ohms) can lead to a weak charge quantization in the superconducting grains. This forbids charge transfer to/from the superconducting regions. The phenomenon effectively disables the superconducting channel in the material by fixing the number of Cooper pairs in the system ($\Delta N = 0$), which results in large phase fluctuations destroying the macroscopic superconducting order⁴⁴.

However, the introduction of superconducting leads in the sample acts as a reservoir of Cooper pairs, bypassing the weak quantization constraint and effectively delocalizing carriers ($\Delta N \neq 0$). This re-enables transport by this network of superconducting islands - thus resulting in the observed behavior in $4p$ measurements.

Our interpretation is also consistent with previous analysis of the magnetic-field-induced metal-insulator transition taking place in HOPG, which indicated intrinsic $2e$ carriers in the material¹³. In particular, the characteristic magnetic field $B_0 \approx 0.13\ \text{T}$ related to the suppression of the $4p$ transition (fig. 3), is very close to the critical magnetic field $B_{crit} \approx 0.11\ \text{T}$ associated with the suppression of the bosonic character of carriers in the system¹³. The presence of paired electrons in the absence of a coherent superconducting phase entails the existence of localized superconducting puddles. Hence, if the $4p$ transition is to be related to small superconducting-prone regions, its suppression should occur in tandem with the suppression of the Bose-metal phase discussed for graphite¹³. This is indeed suggested by the similarity between B_0 obtained here and the parameter B_{crit} of ref. 13.

In the context of thick S-N-S junctions, the characteristic magnetic field $B_0 \approx 0.13\ \text{T}$ (see fig. 3 and the asso-

ciated discussion) can be further related to a distance L between superconducting regions within graphite. This distance can be estimated as²⁹ $L = 2\sqrt{\hbar/(2\pi eB_0)} \approx 100$ nm. Such a value is justified by considering that low magnetic fields (prior to the suppression of superconductivity at the electrodes) disrupt the interaction between superconducting grains within graphite, rather than a macroscopic weak link between the two superconducting electrodes. Random in nature, such grains are to present a sample-dependent distribution. Hinging on their size and coupling, their network can act either as a low- or a high-resistance channel for carriers, akin to observations in homogeneous and highly granular superconducting thin films, respectively⁴⁶.

Although not showing signs of a superconducting gap, STM measurements allow for a second, upper limit estimation of the average distance between such grains. A proximity-induced superconducting gap in a N layer of thickness L is expected to be at least 3 times larger than the structure's Thouless energy^{47,48} $E_{Th} = \hbar D/L^2$. In it, D is the electronic diffusion coefficient on N. For graphite with electronic mobility¹¹ $\mu \approx 10^5$ cm²/V.s, $D \approx 100$ cm²/s at $T = 1$ K. Assuming $E_{Th} \lesssim 5 \times 10^{-4}$ meV in our samples (the experimental resolution) results in an estimated distance between superconducting puddles on graphite of the order $L \approx 1$ μ m. In multi-graphenes, proximity phenomena have been shown to surpass these distances⁴⁹.

The remaining issue becomes, then, the identification of such regions. The absence of clear evidence of superconducting gaps in STM scans seem to discard most of the features commonly found in the surface of graphite (e.g. wrinkles, folds, bubbles, impurities and grain boundaries) as possible candidates for hosting the proposed superconducting-prone regions. We are not able to eliminate, however, regions with gap-like structures in their STS (see fig. 7). These can be associated with the twisting of adjacent graphene layers by small angles³². Such regions been demonstrated to host superconductivity at low temperatures. However, STM measurements specifically designed to probe their properties are yet to reveal clear evidence of superconducting gaps at temperatures as low as 1 K (see e.g. refs. 50,51).

Additionally, experiments performed by us in samples contacted at their lateral edges (see fig. 5) have shown resistance drops below T_c , amounting for about 10% of the total measured signal. Transitions on this geometry were better-defined and larger than those observed on samples contacted at the top surface - figs. 2 and 5). Edge re-

gions are more susceptible to deformations during the sample cutting process, which generate different types of irregularities. Enhanced transitions observed along them further indicate lattice distortions as possible candidates for the phenomenon at hand. Unfortunately, due to the disordered nature of graphite's edges, we are currently unable to probe their differential conductance (as done for the remainder of the sample surface).

In short, we demonstrated the induction of a macroscopic, long-range, superconducting - like proximity effect in bulk graphite outfitted with superconducting current leads. The phenomenon manifests as SC-like transitions on graphite's resistance, which was probed 700 μ m - 1 mm away from the superconducting electrodes (much above $\xi_N \approx 1 - 2$ μ m). The suppression of these transitions is closely related to the breakdown of superconductivity on the current probes, thus suggesting that an unconventional superconducting proximity effect is at play. Our work supports the existence of intrinsic superconducting correlations in low-dimensional, localized regions of pristine graphite. Unfortunately, structural traits responsible for such properties could not be pinned from our measurements. However, results seem to discard features commonly found in the surface of graphite as their source. Our observations open routes towards superconducting electronic circuitry in bulk materials regardless of their volumetric conductivity.

Acknowledgments

We would like to thank Marta Cieplak, A. E. Koshelev, V. M. Vinokur, G. Baskaran and V. Khodel for fruitful discussions. This work was supported by the National Science Center, Poland, research project no. 2016/23/P/ST3/03514 within the The POLONEZ programme. The POLONEZ programme has received funding from the European Union's Horizon 2020 research and innovation programme under the Marie Skłodowska-Curie grant agreement No. 665778. P.G. acknowledges the support of the National Science Center, Poland, research project no. 2014/15/B/ST3/03889. Y.K. was supported by FAPESP, CNPq and AFOSR Grant FA9550-17-1-0132. The research of B.C., P. Sz. and M. K. performed in Slovakia was supported by European Microkelvin Platform (EU's H2020 project under grant agreement no. 824109) and projects VA SR ITMS2014+ 313011W856, APVV-18-0358, VEGA 1/0743/19.

* b.c.camargo@yahoo.com.br

¹ P. G. De Gennes, Rev. Mod. Phys. **36**, 225 (1964).

² I. Bozovic, G. Logvenov, M. A. J. Verhoeven, P. Caputo, E. Goldobin, and M. R. Beasley, Phys. Rev. Lett. **93**, 157002 (2004).

³ R. S. Decca, H. D. Drew, E. Osquiguil, B. Maiorov, and

J. Guimpel, Phys. Rev. Lett. **85**, 3708 (2000).

⁴ D. Marchand, L. Covaci, M. Berciu, and M. Franz, Phys. Rev. Lett. **101**, 097004 (2008).

⁵ J. E. Sadleir, S. J. Smith, I. K. Robinson, F. M. Finkbeiner, J. A. Chervenak, S. R. Bandler, M. E. Eckart, and C. A. Kilbourne, Phys. Rev. B **84**, 184502 (2011).

- ⁶ J. E. Sadleir, S. J. Smith, S. R. Bandler, J. A. Chervenak, and J. R. Clem, *Phys. Rev. Lett.* **104**, 047003 (2010).
- ⁷ T. Klapwijk, G. Blonder, and M. Tinkham, *Physica B+C* **109-110**, 1657 (1982).
- ⁸ I. O. Kulik, *SOVIET PHYSICS JETP* **30**, 944 (1970).
- ⁹ S. Zhou, G. Gweon, J. Graf, A. Fedorov, C. Spataru, R. Diehl, Y. Kopelevich, D. Lee, S. Louie, and A. Lanzara, *Nature Physics* **2**, 595 (2006).
- ¹⁰ N. García, P. Esquinazi, J. Barzola-Quiquia, B. Ming, and D. Spodig, *Phys. Rev. B* **78**, 035413 (2008).
- ¹¹ B. C. Camargo, Y. Kopelevich, A. Usher, and S. B. Hubbard, *Applied Physics Letters* **108**, 031604 (2016), <https://doi.org/10.1063/1.4940233>.
- ¹² K. Antonowicz, *Nature* **247**, 358 (1974).
- ¹³ Y. Kopelevich, P. Esquinazi, J. Torres, R. Silva, and H. Kempa, "Advances in solid state physics," (Springer, 2003) Chap. Graphite as a Highly Correlated Electron Liquid.
- ¹⁴ S. G. Lebedev, *Journal of Physics and Chemistry of Solids* **75**, 1029 (2014).
- ¹⁵ A. Ballestar, P. Esquinazi, and W. Böhlmann, *Phys. Rev. B* **91**, 014502 (2015).
- ¹⁶ Y. Kopelevich, J. C. M. Pantoja, R. R. da Silva, and S. Moehlecke, *Phys. Rev. B* **73**, 165128 (2006).
- ¹⁷ Y. Kopelevich, P. Esquinazi, J. Torres, and S. Moehlecke, *Journal of Low Temperature Physics* **119**, 691 (2000).
- ¹⁸ Y. Cao, V. Fatemi, S. Fang, K. Watanabe, T. Takashi, E. Kaxiras, and P. Herrero, *Nature* **556**, 43 (2018).
- ¹⁹ X. Liu, Z. Hao, E. Khalaf, J. Lee, K. Watanabe, T. Taniguchi, A. Vishwanath, and P. Kim, *arXiv:1903.08130* (2019).
- ²⁰ M. Hayashi, H. Yoshioka, and A. Kanda, *Journal of Physics: Conference Series* **109**, 012014 (2008).
- ²¹ T. Sato, A. Kanda, T. Moriki, H. Goto, S. Tanaka, Y. Ootuka, H. Miyazaki, S. Odaka, K. Tsukagoshi, and Y. Aoyagi, *Physica C: Superconductivity and its Applications* **468**, 797 (2008), proceedings of the Fifth International Conference on Vortex Matter in Nanostructured Superconductors.
- ²² G.-H. Lee and H.-J. Lee, *Applied Physics Express* **6**, 025102 (2013).
- ²³ T. Sato, T. Moriki, S. Tanaka, A. Kanda, H. Goto, H. Miyazaki, S. Odaka, Y. Ootuka, K. Tsukagoshi, and Y. Aoyagi, *Physica E: Low-dimensional Systems and Nanostructures* **40**, 1495 (2008).
- ²⁴ S. Sangiao, L. Casado, L. Morellón, M. R. Ibarra, and J. M. D. Teresa, *Journal of Physics D: Applied Physics* **50**, 12LT02 (2017).
- ²⁵ (2019), Beijing Great Wall Co. Ltd. No.10 Ronghua South Road 100176 Beijing, China.
- ²⁶ B. T. Kelly, *Physics of graphite* (London: Applied Science Publishers, 1981).
- ²⁷ X. Du, S.-W. Tsai, D. L. Maslov, and A. F. Hebard, *Phys. Rev. Lett.* **94**, 166601 (2005).
- ²⁸ T. Hamada, K. Yamakawa, and F. E. Fujita, *Journal of Physics F: Metal Physics* **11**, 657 (1981).
- ²⁹ L. Dobrosavljevic-Grujic and Z. Radovic, *Supercond. Sci Tech.* **6** (1993).
- ³⁰ Z. Han, A. Adrien, H. Tash, K. Tikhonov, M. Feigelman, B. Sacepe, and V. Bouchiat, *Nature Physics* **10**, 380 (2014).
- ³¹ M. Kompaniets, O. V. Dobrovolskiy, C. Neetzel, E. Begun, F. Porrati, W. Ensinger, and M. Huth, *Journal of Applied Physics* **116**, 073906 (2014), <https://doi.org/10.1063/1.4893549>.
- ³² E. Y. Andrei, G. Li, and X. Du, *Reports on Progress in Physics* **75**, 056501 (2012).
- ³³ M. Yankowitz, S. Chen, H. Polshyn, K. Watanabe, T. Taniguchi, D. Graf, A. F. Young, and C. R. Dean, *arXiv:1808.07865v2 [cond-mat.mes-hall]* (2018).
- ³⁴ A. Pleceník, M. Grajcar, i. c. v. Beňačka, P. Seidel, and A. Pfuch, *Phys. Rev. B* **49**, 10016 (1994).
- ³⁵ D. D. L. Chung, *Journal of Materials Science* **37**, 1475 (2002).
- ³⁶ Y. Kobayashi, K.-i. Fukui, T. Enoki, K. Kusakabe, and Y. Komiya, *Phys. Rev. B* **71**, 193406 (2005).
- ³⁷ A. B. Pippard and R. G. Chambers, *Proceedings of the Physical Society of London, Section A* **65**, 955 (1952).
- ³⁸ V. Beletskii, A. Golik, A. Korolyuk, and M. Obolenskii, *Zh. Eksp. Teor. Fiz.* **69**, 1045 (1975).
- ³⁹ V. Gantmakher and V. Dolgoplov, *Zh. Eksp. Teor. Fiz* **60**, 2260 (1971).
- ⁴⁰ C. Precker, P. Esquinazi, A. Champi, J. B. Quiquia, M. Zoraghi, S. M. Lanfin, A. Setzer, W. Bohlmann, D. Spemann, J. Meijer, T. Muenster, O. Baehre, G. Kloess, and H. Beth, *New Journal of Physics* **18**, 113041 (2016).
- ⁴¹ G. Deutscher, *Nature* **397**, 410 (1999).
- ⁴² D. E. Soule, *Phys. Rev.* **112**, 698 (1958).
- ⁴³ H. Kempa, P. Esquinazi, and Y. Kopelevich, *Phys. Rev. B* **65**, 241101 (2002).
- ⁴⁴ M. V. Feigel'man, A. I. Larkin, and M. A. Skvortsov, *Phys. Rev. Lett.* **86**, 1869 (2001).
- ⁴⁵ (2008), V. Feigelman, A. Kamenev, A. I. Larkin, and M. A. Skvortsov, *Phys. Rev. B* **66**, 054502 (2002).
- ⁴⁶ A. Goldman, *Physica E: Low-dimensional Systems and Nanostructures* **23rd International Conference on Low Temperature Physics (LT23)**.
- ⁴⁷ H. le Sueur, P. Joyez, H. Pothier, C. Urbina, and D. Esteve, *Phys. Rev. Lett.* **100**, 197002 (2008).
- ⁴⁸ T. Quaglio, F. Dahlem, S. Martin, A. Gérardin, W. Winkelmann, and H. Courtois, *Review of Scientific Instruments* **83**, 123702 (2012), <https://doi.org/10.1063/1.4769258>.
- ⁴⁹ H. Heersche, P. Herrero, J. Oostinga, L. Vandersypen, and A. Morpurgo, *Nature* **466**, 56 (2007).
- ⁵⁰ Y. Jiang, X. Lai, K. Watanabe, T. Taniguchi, K. Haule, J. Mao, and E. Andrei, *Nature* **573**, 91 (2019).
- ⁵¹ Y. Xie, B. Lian, B. Jack, X. Liu, C. Chi, K. Watanabe, T. Taniguchi, B. Bernevig, and A. Yazdani, *Nature letters* **572**, 101 (2019).